Thermal neutron detectors based on hexagonal boron nitride epilayers

T. C. Doan, A. Marty, J. Li, J. Y. Lin, and H. X. Jiang
Department of Electrical and Computer Engineering, Texas Tech University, Lubbock, TX 79409

ABSTRACT

Solid-state neutron detectors with high performances are urgently sought after for the detection of fissile materials. Until now, direct-conversion neutron detectors based on semiconductors with a measureable efficiency have not been realized. We have successfully synthesized hexagonal boron nitride (*h*-BN) epilayers with varying thicknesses (0.3 μm – 50 μm) by metal organic chemical vapor deposition (MOCVD) on sapphire substrates. In this paper, we present the detailed characterization of thermal neutron detectors fabricated from *h*-BN epilayers with a thickness up to 5 μm to obtain insights into the *h*-BN epilayer thickness dependence of the device performance. The results revealed that the charge collection efficiency is almost independent of the *h*-BN epilayer thickness. By minimizing *h*-BN material removal by dry etching, it was shown that detectors incorporating an isotopically ^{10}B-enriched *h*-BN epilayer of 2.7 μm in thickness exhibited an overall detection efficiency for thermal neutrons of 4% and a charge collection efficiency as high as 83%. By doing away altogether with dry etching, we have successfully realized a simple vertical 43 μm thick *h*-^{10}BN detector which delivers a detection efficiency of 51.4% for thermal neutrons, which is the highest reported efficiency for any semiconductor-based neutron detector The *h*-BN detectors possess all the advantages of semiconductor devices including low cost, high efficiency and sensitivity, wafer-scale processing, compact size, light weight, and ability to integrate with other functional devices.

Key words: Hexagonal boron nitride, solid-state neutron detectors, direct-conversion neutron detectors, wide bandgap semiconductors.

1. INTRODUCTION

Neutron detectors with improved detection efficiency are highly useful for a range of applications including fissile materials sensing, neutron therapy, medical imaging, probing of crystal structures, and oil exploration. Presently, the most dominant detection technology is based on ^{3}He gas-filled devices with the major advantages of intrinsically low background count and high detection efficiency. Some of the disadvantages of ^{3}He gas-filled detectors include high cost due to the shortage of ^{3}He gas, slow response (10 - 100 μs) and a relative lack of flexibility in configuring the bulky ^{3}He gas tube based systems. The development of alternative detection technologies that do not require the use of ^{3}He gas will enable the researchers and users to dedicate the scarce supplies of ^{3}He gas to other applications where no substitutes are possible [1,2].

The element B has been identified as one of the most attractive alternative materials because of the very high thermal neutron cross-section (~3840 barns) of its B-10 (^{10}B) isotope [3,4]. Among the B-based semiconductors, boron nitride (BN) has been the material of choice [5,6] due to its outstanding material properties including high thermal conductivity, large energy band gap ($E_g \approx 6.5$ eV), high resistivity and excellent electrical transport properties. BN exists in several crystalline forms including hexagonal, cubic, *wurtzite,* rhombohedral, and turbostratic [7-10]. The sp^2-bonded hexagonal form, hexagonal BN (*h*-BN), is the most stable phase when synthesized at any temperature under ambient pressure [7-10]. Due to its simpler crystal structure than other B-based compounds such as B_4C [11,12], $B_{12}As_2$ [13], and $B_{12}P_2$ [14], it is possible to synthesis single crystalline *h*-BN films (or epilayers) by standard epitaxial growth techniques such as metal organic chemical vapor deposition (MOCVD) [15-23]. Materials with single crystalline structure contain fewer charge traps than polycrystalline or amorphous materials and enable more efficient

Hard X-Ray, Gamma-Ray, and Neutron Detector Physics XVIII, edited by Ralph B. James, Michael Fiederle, Arnold Burger, Larry Franks, Stephen A. Payne, Proc. of SPIE Vol. 9968, 99680S · © 2016 SPIE · CCC code: 0277-786X/16/$18 · doi: 10.1117/12.2239079

charge collection efficiency. Recent experimental studies have indicated that *h*-BN thin films are highly promising for the fabrication of solid-state neutron detectors [21-23]. When a ^{10}B atom captures a thermal neutron, it undergoes the following nuclear reaction [3]:

$$^{1}_{0}\mathrm{n} + {}^{10}_{5}\mathrm{B} \rightarrow {}^{4}_{2}\alpha^{*}(1.47\mathrm{MeV}) + {}^{7}_{3}\mathrm{Li}^{*}(0.84\mathrm{MeV}) \ (94\%), \quad (1a)$$

$$^{1}_{0}\mathrm{n} + {}^{10}_{5}\mathrm{B} \rightarrow {}^{4}_{2}\alpha(1.77\mathrm{MeV}) + {}^{7}_{3}\mathrm{Li} \ (1.015\mathrm{MeV})(6\%). \quad (1b)$$

The energies released from the nuclear reactions are in the form of kinetic energies of daughter particles, alpha (α) and lithium (^{7}Li). These particles have a range of about 5 μm and 2 μm respectively for α and ^{7}Li in isotopically ^{10}B enriched *h*-BN [3,6] and deposit their kinetic energies to generate electron–hole pairs inside the *h*-BN semiconductor. The collection of these electrons and holes serves as the detection signal for neutrons. In *h*-BN neutron detectors, the neutron capture, nuclear reaction, electrical charge collection and signal generation all occur in the same *h*-BN layer. This is in contrast to boron coated or perforated indirect conversion devices [24-27], in which the thermal neutron absorption and nuclear reaction take place in the boron layer of micro-filling regions, ^{7}Li and α particles created at the nuclear reaction site have to travel a certain distance before they reach (or never reach) the semiconductor layer to generate electrons and holes. Thus, *h*-BN detectors are direct conversion detectors and potentially capable of providing a higher detection efficiency and higher energy resolution of the reaction products than those of the indirect conversion devices. Furthermore, the ability of producing wafer scale *h*-BN materials by epitaxial growth techniques and the easy adoption of semiconductor processing technologies offer the possibility to make neutron detectors with many unique advantages with the potential to provide portable neutron detectors as well as to replace ^{3}He gas detectors at radiation portal monitors. The other unique attribute of *h*-BN detectors is that they have a negligible response to γ-photons because BN is composed of low atomic number elements, B and N [22].

Until now, *h*-BN neutron detectors were fabricated from thin natural *h*-BN epilayers (around 1 μm in thickness) [21-23], in which isotope ^{10}B is about 20% and isotope ^{11}B is about 80% [3,4]. The use of thin natural *h*-BN layers has limited ability to evaluate the overall detection efficiency as well as the charge collection efficiency of *h*-BN thin film detectors. More recently, we have successfully developed MOCVD growth processes for obtaining *h*-BN with large thickness (~50 μm). In this work, we report the detailed device fabrication and characterization for neutron detectors which incorporate *h*-BN epilayers with a thickness up to 5 μm to provide insights into the charge collection efficiency and device design optimization. We have demonstrated that detectors incorporating ^{10}B-enriched *h*-BN epilayers with a thickness of 2.7 μm have an overall detection efficiency for thermal neutrons of 4% and a charge collection efficiency as high as 83%. The results indicate that the charge collection efficiency of *h*-BN detectors is almost independent of the wafer thickness, whereas dry etching potentially introduces defects which have an impact on the charge collection efficiency. The present results represent a significant step towards the realization of high efficiency solid-state thermal neutron detectors based on *h*-BN with expected advantages resulting from semiconductor technologies, including compact size, light weight, low cost, high efficiency and sensitivity, and ability to integrate with other functional devices.

2. EXPERIMENT

Hexagonal BN has a close lattice match to graphite, high thermal and chemical stability, and high corrosion resistance and is being recognized as the most suitable substrate/dielectric/separation layer for two-dimensional electronics and optoelectronics [28-31]. As such, much efforts in the synthesis of *h*-BN have been largely focused on mono- or a few layers of *h*-BN in the past [29]. However, the attainment of *h*-BN epilayers with large thicknesses is highly desirable for practical applications in neutron detectors because the number of electron-hole pairs generated in *h*-BN and hence the overall detection efficiency depend on the thickness of *h*-BN owing to the fact that the number of absorbed neutrons increases with the *h*-BN layer thickness. The boron density in natural *h*-BN is about 5.5×10^{22} cm^{-3} in which isotope ^{10}B is about 20% and isotope ^{11}B is about 80% [3,4]. Therefore, the density of isotope ^{10}B atoms in natural *h*-BN is about N =

$1.1x10^{22}$ cm^{-3}. This gives a microscopic neutron absorption coefficient (α) and absorption length (λ) in a natural *h*-BN to be: $\alpha=N\sigma=42.24$ cm^{-1} and $\lambda=\frac{1}{\alpha}=2.37x10^{-2}\,cm=237\,\mu m$, where σ (= 3840 barns = $3.84x10^{-21}$ cm^2) is the cross section of ^{10}B for 25 meV thermal neutrons. For pure isotopically ^{10}B-enriched *h*-BN (*h*-^{10}BN), the thermal neutron absorption coefficient will be a factor of 5 larger, making the thermal neutron absorption length a factor of 5 smaller. Thus, we have λ=47 μm for *h*-^{10}BN. The absorption lengths of thermal neutrons in natural and ^{10}B-enriched *h*-BN epilayers are several orders of magnitude smaller than that in ^3He gas. Nevertheless, realizing *h*-BN epilayers with high crystalline quality as well as with sufficient thickness is quite challenging due to the strong bonds between B-N in the basal plane, the slow surface diffusion of B atoms, and the strong parasitic chemical reaction between the boron and nitrogen precursors

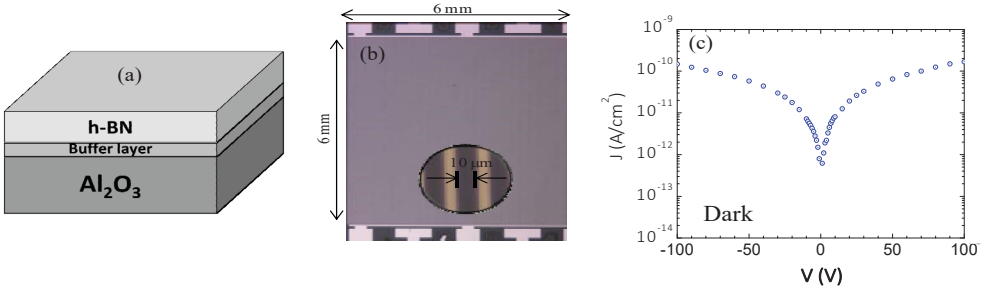

Fig. 1 (a) Schematic layer structure of h-BN epilayers used for neutron detector fabrication. (b) Optical image of a fabricated h-BN metal-semiconductor-metal (MSM) detector with a device size of 6 mm x 6 mm and the widths of etched trenches and micro-strips of 10 μm and 10 μm, respectively. (c) Typical dark I-V characteristic (leakage current density vs. applied bias voltage) of h-BN MSM detectors.

during the growth.

In this work, we have employed low pressure MOCVD growth technique to synthesis *h*-BN epilayers. The layer structure is schematically shown in Fig. 1(a). The precursors for boron and nitrogen are triethylboron (TEB) and ammonia (NH_3), respectively. Hydrogen was used as a carrier gas. A pulsed growth scheme (alternating flows of TEB and NH_3) was undertaken to minimize the pre-reaction between TEB and ammonia [32,33], which is very important for obtaining epilayers in hexagonal phase. Furthermore, it was found that the photoluminescence emission intensity associated with the nitrogen vacancy (V_N) related point defects decreases exponentially with increasing the NH_3 flow rate [34]. As the NH_3 flow rate increases, more N atoms are supplied to the reaction zone and hence the concentrations of V_N and its related defects in the samples are decreased. Thus conducting the growth in N-rich conditions is critical to minimizing the density of V_N and V_N related defects, which act as charge traps. Moreover, due to the lattice mismatch between *h*-BN and Al_2O_3, a low temperature BN buffer layer of about 10 nm in thickness was deposited on the sapphire substrate prior to the growth of *h*-BN epilayer. We have studied the impact of this buffer layer thickness on the quality of the epilayers and have arrived at ~10 nm as the optimum buffer layer thickness required to grow better quality *h*-BN epilayers. The growth temperature used to produce *h*-BN epilayers reported in this work was between 1300 °C – 1350 °C. The observed linewidth of the x-ray diffraction rocking curve (ω-scan) of the *h*-BN (0002) diffraction peak is around 380 arcsec [23] and is one order of magnitude narrower than those of previously reported values (1.5-0.7 degrees or 5400-2520 arcsec) for ultra-thin layers [15,20].

Thermal neutron detectors based on metal-semiconductor-metal (MSM) architecture with micro-strip interdigital fingers were fabricated from *h*-BN epilayers, aiming to take advantage of the excellent lateral transport properties of *h*-BN epilayers. The photolithography technique was used to pattern the interdigital fingers on the surface of *h*-BN epilayers. The pattern transfer was accomplished using a sulfur hexafluoride (SF_6) gas-based inductively-coupled plasma (ICP) dry etching [35,36]. The patterns were etched all the way to the sapphire substrate. Metal contacts consisting of bi-layers of Ti/Al (20 nm/30 nm) were deposited by e-beam evaporation. Figure 1(b) is a micrograph of a representative *h*-BN MSM detector having an epilayer

thickness of 4.5 μm, a dimension of 6 mm x 6 mm, and the widths of etched trenches and micro-strips of 10 μm and 10 μm, respectively.

3. RESULTS AND DISCUSSIONS

3.1. Natural *h*-BN detectors

Owing to its wide bandgap, undoped *h*-BN epilayers are highly insulating. As such, *h*-BN detectors exhibit extremely small leakage current density. This is demonstrated in Fig. 1(c), where the dark I-V characteristic (leakage current density vs. applied bias voltage) of a fabricated *h*-BN detector is shown. For instance, at a voltage of 10 V, the leakage current density is below 10^{-11} A/cm^2, which is about 5 orders of magnitude lower than that of the-state-of-the-art micro-structured Si detectors filled with boron-10 [27].

To characterize the thermal neutron response, a depleted sealed source of californium-252 (^{252}Cf) (from

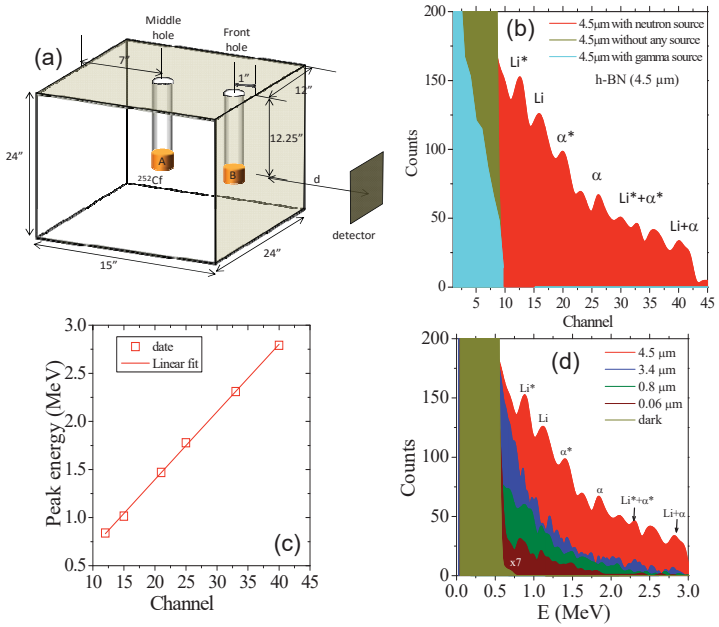

Fig. 2 (a) Schematic diagram of thermal neutron source consisting of a ^{252}Cf source in conjunction with a moderator constructed from a high density polyethylene (HDPE) block. (b) Nuclear reaction pulse height spectrum (counts versus channel number) obtained by a natural *h*-BN MSM neutron detector of 4.5 μm in thickness. (c) Energy peak calibration among the nuclear reaction products expected from Eq. (1). (d) Nuclear reaction pulse height spectra measured by natural *h*-BN MSM neutron detectors of varying h-BN layer thicknesses. The detectors were placed at a distance of *d*=9 cm away from the front surface of the HDPE moderator. Dark yellow is the background counts; and other colors represent counts obtained from h-BN detectors with different layer thicknesses (*t*) in response the thermal neutron source.

Frontier Technology) was used as a neutron source and the associated detection electronics include a charge sensitive preamplifier, pulse shaping amplifier, and multi-channel analyzer. As schematically illustrated in Fig. 2(a), a high density polyethylene (HDPE) moderator was constructed for two purposes: (1) for moderating the fast neutrons to thermal neutrons and (2) for the storage of the ^{252}Cf source [27,42]. If the neutron source was placed at the position "A", most fast neutrons are stopped by the HDPE moderator. If the neutron source was placed at the position "B", neutrons emerging from the front surface of the HDPE moderator are mostly thermal neutrons (neutrons with a kinetic energy ranging from 1 to 100 meV with a spectral peak at 25 meV). The detectors were placed inside a metal box to minimize electronic noise and at a distance of *d*=9 cm away from the front surface of the HDPE moderator. By conducting the pulse-height

spectra measurements at varying distances from the ^{252}Cf, we found that the distance *d*=9 cm (from the front surface of the HDPE moderator) provides an appropriate compromise between minimizing the pile-up effect and ensuring a sufficient thermal neutron flux. Monte Carlo N particle code simulations together with the point source model [42] provided that the flux of the thermal neutrons at 9 cm away from the front surface of the HDPE moderator a flux of 2 x 10^3 (thermal neutron/cm^2·s). The pulse-height spectra of the thermal neutron and ^{10}B reaction product were measured by *h*-BN detectors for a total counting time of 1200 s.

The measured pulse-height spectrum of the 4.5 μm thick detector is shown in Fig. 2(b), which exhibits very well resolved peaks corresponding to all the product energies of ^{10}B and thermal neutron reaction described in Eq. (1), including Li, Li*, α, and α* peaks as well as the sum peaks Li + α and Li* + α*, as we have demonstrated previously [23]. The calibration between the energy and channel number for the whole spectrum of the 4.5 μm thick detector is plotted in Fig. 2(c), which shows a linear relationship between the reaction product energies of Li*, Li, α*, α, Li* + α*, and Li + α peaks and the channel numbers, exactly corresponding to the values expected from Eq. (1). The open squares in Fig. 2(c) are the data points and the solid line is the linear fit. This agreement between the experimental data and expected energy peaks of the nuclear reaction products of Eq. (1) shown in Fig. 2(c) provides an assurance in our assignment of the observed peaks in the pulse-height spectra. In Fig. 2(d), the pulse height spectra are plotted in the energy scale for *h*-BN detectors with different layer thicknesses. The dark yellow curve is the background counts obtained in the absence of the neutron source attributed to the electronic circuit noise; curves of other colors represent counts obtained from *h*-BN detectors with different epilayer thicknesses under the irradiation of thermal neutrons.

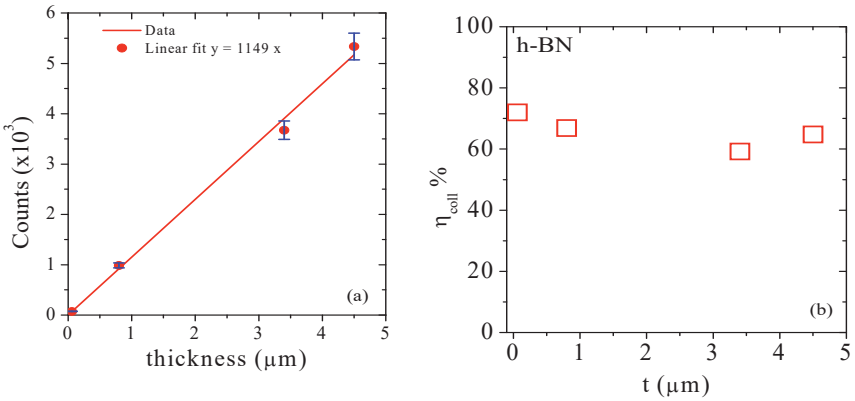

Fig. 3 (a) Measured counts as a function of the layer thickness, t, of natural h-BN detectors. (b) Experimentally deduced charge collection efficiency (η_{coll}) as a function of t according Eq. (3).

The total number of thermal neutrons irradiating on the detector (with a device area of A = 0.6 x 0.6 = 0.36 cm^2) during 1200 s irradiation time is N_{in} = ΦA·(counting time) = 8.64 x 10^5, while the number of absorbed thermal neutrons depends on the thickness of *h*-BN epilayers. The probability of interaction (P) between the thermal neutrons and *h*-BN epilayers follows

$$P = 1 - \exp(-\frac{t}{\lambda}) \approx \frac{t}{\lambda}, \qquad \text{if } t << \lambda, \tag{2}$$

where λ (=237 μm) is a thermal neutron absorption length of natural *h*-BN and *t* is the *h*-BN epilayer thickness. Equation (2) indicates that for thin epilayers ($t << \lambda$), the interaction probability increases linearly with the layer thickness (*t*). Figure 3 (a) plots the measured counts (N_C) as a function of the *h*-BN epilayer thickness. The result presented in Fig. 3 (a) clearly shows that N_C increases linearly with the *h*-BN epilayer thickness as expected from Eq. (2). The slope in Fig. 3 (a) is a measure of total counts per unit thickness (in μm), CR_m=1149 (μm)$^{-1}$. The expected counting rate can be calculated according to N_{in}·P ≈ N_{in}·(t/λ), from

which the expected total counts per unit thickness is CR_m=8.64 x 10^5/237 μm=3646 $(\mu m)^{-1}$. The discrepancy between the measured total counts per unit thickness (CR_m = 1149/μm) and the expected value (CR_e = 3646/μm) is due to the fact that half of the *h*-BN detection area was etched away for metal contact deposition in the specific MSM device geometry employed in Fig. 1 (b) and that the charge collection efficiency is not 100%.

The charge collection efficiency (η_{coll}) is one of the most important parameters of a radiation detector and knowing this parameter is highly useful to the further development of *h*-BN materials and devices since this parameter depends on the overall material quality. This parameter is defined as the ratio of the measured detection efficiency ($\eta=N_C/N_{in}$) to the interaction probability (P) according to the following,

$$\eta_{coll} = \frac{\eta}{P} = \frac{N_C}{N_{in} \cdot \frac{t}{\lambda}}, \qquad (3)$$

where N_C is the measured counts and N_{in} is the total number of thermal neutrons irradiating on the detector. Figure 3 (b) plots the charge collection efficiency (η_{coll}) as a function of the *h*-BN detector thickness (*t*) according to Eq. (3). In plotting Fig. 3(b), a fraction of 0.5 was included in the interaction probability (P) to account for the fact that half of the *h*-BN detection area was etched away for this set of devices. The result shows that the charge collection efficiency of *h*-BN detectors is about 70%, almost independent of the *h*-BN layer thickness. Such a high charge collection efficiency is a result of the single crystalline nature. However, the overall detection efficiency (η) of this set of *h*-BN detectors is below 1% because these devices incorporated natural *h*-BN epilayers with thicknesses less than 5 μm and 50% of the detection area is removed in the MSM detector design shown in Fig. 1 (b).

3.2. ^{10}B isotopically enriched *h*-BN detectors

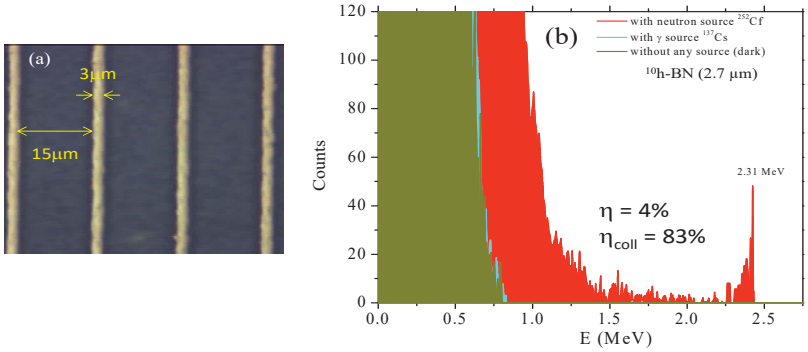

Fig. 4 (a) Optical image of a portion of an MSM detector fabricated from isotopically ^{10}B-enriched h-BN epilayer (h-^{10}BN) of 2.7 μm in thickness. The detector has a dimension of 25 mm^2 (5 mm x 5 mm) and the widths of etched trenches and micro-strips of 3 μm and 15 μm, respectively. (b) Nuclear reaction pulse height spectrum measured by the h-^{10}BN MSM detector of Fig. 4 (a) for 10 minutes using the same thermal neutron source setup shown in Fig. 2 (a).

One of the most effective ways to increase neutron detection efficiency is by ^{10}B isotopic enrichment of the source molecules, which can increase the neutron absorption efficiency by a factor of 5 with little or no impact on the semiconducting properties. By adopting the growth processes established for natural *h*-BN, we have successfully produced isotopically ^{10}B-enriched *h*-BN (*h*-^{10}BN) epilayers with a thickness as large as 50 μm. Here, report results for devices incorporating of a 2.7 μm *h*-^{10}BN epilayer. The ^{10}*h*-BN MSM detectors were fabricated using the same device processing procedures as those of *h*-BN detectors with the exception that the *h*-^{10}BN MSM detectors have the micro-strip width of 15 μm and etched trench width of 3 μm in order to reduce the fraction of scarified *h*-^{10}BN materials and maximize the detection area, as illustrated in

Fig. 4 (a). Figure 4 (b) shows a pulse height spectrum of the thermal neutron and ^{10}B reaction product measured by an *h*-^{10}BN detector using the same procedures outlined in the previous sub-section for natural *h*-BN detectors except that the counting time was reduced to 600 s. This gives N_{in} = ΦA·(counting time) = $2 \times 10^3 \times 0.25\,cm^2 \times 600\,s = 3 \times 10^5$. Similar to those of natural *h*-BN detectors, the spectrum retains the unique feature of high energy resolution of the reaction products with the sum peak at 2.31 eV being the most predominant.

The overall detection efficiency of *h*-^{10}BN detectors (with a layer thickness of 2.7 μm) has been determined by two methods. The first method is based on the ratio of the measured counts in response to the thermal neutrons (N_c) to the total number of thermal neutrons irradiating on the detector (N_{in}), $\eta=N_C/N_{in}$, which provides η=4%. The second method is based on the comparison of the relative thermal neutron responses between our *h*-^{10}BN detector and a commercially certified ^6Li filled microstructured Si semiconductor neutron detector (MSND) model D411S-30-D0010-V4 (Domino V4 neutron detector) from Radiation Detection Technologies Inc., which has a detection area of 4 cm^2 and a specified absolute detection efficiency of 30% for thermal neutrons. Comparing the total counts detected by MSND and ^{10}*h*-BN detector placed at the same distance from the thermal neutron source and scaling the relative detection area of 4 cm^2 for MSNS vs. 0.25 cm^2 (=5 mm x 5 mm) for *h*-^{10}BN detector, we obtain an absolute detection efficiency of ~4.1% for ^{10}*h*-BN detector, which is in excellent agreement with the value calculated from $\eta=N_C/N_{in}$.

The theoretical thermal neutron absorption length of 100% pure isotopically ^{10}B-enriched *h*-^{10}BN is about 47 μm, which is 5 times shorter than that of natural *h*-BN (237 μm), based on which the expected interaction probability of *h*-^{10}BN detectors (with a layer thickness of 2.7 μm) should be P=4.8%, where $P\approx(t/\lambda)(15/18)=(2.7/47)(15/18)=4.8\%$. Here, the fraction 15/18 is included because the etched trench width is 3 μm and so a fraction of 3/18 of the detection material was removed based on Fig. 4(a). The discrepancy between the measured detection efficiency (η) and the expected interaction probability (P) can be accounted for exactly by the charge collection efficiency (η_{coll}) of *h*-BN detectors, $\eta_{coll} = \eta/P$, which is 83% [42]. The results indicate that the MSM detector design with the micro-strip width of 15 μm and etched trench width of 3 μm shown in Fig. 4(a) adequately addresses the concern of how to maximize the detection area (or minimizing the fraction of removed *h*-^{10}BN materials) and that the charge collection efficiency can be further improved by implementing detector architectures which do not use dry etching process. Indeed, we have recently achieved simple vertical detectors without the use of etching and shown that 43 μm thick *h*-^{10}BN detectors possess a detection efficiency of 51.4% for thermal neutrons, which is the highest reported efficiency for any semiconductor-based neutron detector [43].

4. SUMMARY

In summary, natural and isotopically ^{10}B-enriched *h*-BN epilayers with different thicknesses have been successfully synthesized by MOCVD. These materials were utilized to construct solid-state thermal neutron detectors. The results revealed that the charge collection efficiency of *h*-BN detectors is quite high (around 83%) for devices with reduced etching trenches. Further development of epi-growth processes will likely to produce *h*-BN epilayers with improved material quality and advance the charge collection efficiency to nearly 100%. The ability to synthesis 2-inch (or larger) wafers of *h*-BN epilayers, the applicability of semiconductor processing technologies, and the outstanding attributes of high charge collection efficiency and high energy resolution of the reaction products of *h*-BN detectors, open up new opportunities to construct high efficiency and sensitivity, compact, robust and low cost solid-state neutron detectors.

The efforts on *h*-BN material growth and neutron detectors study are supported by DHS ARI program (No. 2011-DN-077-ARI048) and the studies of the basic optical and structural properties of *h*-BN epilayers are supported by NSF (ECCS-1402886). Jiang and Lin are grateful to the AT&T Foundation for the support of Ed Whitacre and Linda Whitacre endowed chairs.

REFERENCES

[1] H.O. Menlove, D. Henzlova, L.G. Evans, M.T. Swinhoe, and J.B. Marlow, "3He Replacement for Nuclear Safeguards Applications - an Integrated Test Program to Compare Alternative Neutron Detectors," ESARDA 40th Annual Meeting, May 2011.

[2]http://www.dhs.gov/news/2014/07/29/written-testimony-dndo-house-homeland-security-subcommittee-cybersecurity

[3] G. F. Knoll, "Radiation detection and measurement," 4th edition, (John Wiley & Sons, 2010).

[4] O. Osberghaus, Zeitschrift fuer Physik **128**, 366 (1950).

[5] J. Uher, S. Pospisil, V. Linhart, and M. Schiebar, Appl. Phys. Lett. **90**, 124101 (2007).

[6] F. P. Doty, *Boron nitride solid-state neutron detec*tor, US patent, 6,727,504.

[7] R. W. Lynch and H. G. Drickamer, J. Chem. Phys. **44**, 181 (1966).

[8] R. S. Pease, Acta Cryst. **5**, 356 (1952).

[9] Numerical Data and Functional/Relationship in Science and Technology - Crystal and Solid State Physics, edited by Q. Madelung, Landolt-Bornstein Vol. III (Springer, Berlin, 1972).

[10] http://www.ioffe.ru/SVA/NSM/Semicond/.

[11] K. Osberg, N. Schemm, S. Balkir, J. O. Brand, M. S. Hallbeck, P. A. Dowben, and M. W. Hoffman, IEEE Sensor J. **6**, 1531 (2006).

[12] E. Echeverría, R. James, U. Chiluwal, F. L. Pasquale, J. A. Colón Santana, R. Gapfizi, J. D. Tae, M. S. Driver, A. Enders, J. A. Kelber, and P. A. Dowben, Appl. Phys. A, 118, 113 (2015).

[13] J. W. Pomeroy, M. Kuball, H. Hubel, N. W. A. van Uden, D. J. Dunstan, R. Nagarajan, and J. H. Edgar, J. Appl. Phys. **96** 910 (2004).

[14] J. O. Schmitt, J. H. Edgar, L. Liu, T. Szyszko, S. Podsiadlo, and G. Wojciech, Physica Status Solidi C, **2** 1077 (2005).

[15] Y. Kobayashi, T. Akasaka, and T. Makimoto, J. Cryst. Growth **310**, 5048 (2008).

[16] R. Dahal, J. Li, S. Majety, B.N. Pantha, X. K. Cao, J. Y. Lin, and H. X. Jiang, Appl. Phys. Lett. **98**, 211110 (2011).

[17] J. Li, S. Majety, R. Dahal, W. P. Zhao, J. Y. Lin, and H. X. Jiang, Appl. Phys. Lett. **101**, 171112 (2012).

[18] S. Majety, X. K. Cao, J. Li, R. Dahal, J. Y. Lin, and H. X. Jiang, Appl. Phys. Lett. **101**, 051110 (2012).

[19] Y. Kobayashi, K. Kumakura, T. Akasaka, and T. Makimoto, Nature **484** 223 (2012).

[20] M. Chubarov, H. Pedersen, H. Högberg, S. Filippov, J. A. A. Engelbrecht, J. O'Connel, A. Henry, Physica B **439**, 29 (2014).

[21] J. Li, R. Dahal, S. Majety, J. Y. Lin, and H. X. Jiang, Nucl. Instr. Meth. Phys. Res. A **654**, 417 (2011).

[22] T. C. Doan, S. Majety, S. Grendadier, J. Li, J. Y. Lin, and H. X. Jiang, Nucl. Instr. Meth. Phys. Res. A, **748**, 84 (2014).

[23] T. C. Doan, S. Majety, S. Grendadier, J. Li, J. Y. Lin, and H. X. Jiang, Nucl. Instr. Meth. Phys. Res. A, **783**, 121 (2015).

[24] J. Nikolic, A. M. Conway, C. E. Reinhardt, R. T. Graff, T. F. Wang, N. Deo, and C. L. Cheung, Appl. Phys. Lett. **93**, 133502 (2008).

[25] Q. Shao, L. F. Voss, A. M. Conway, R. J. Nikolic, M. A. Dar and C. L. Cheung, Appl. Phys. Lett. **102**, 063505 (2013).

[26] S. L. Bellinger, W. J. McNeil, T. C. Unruh, D. S. McGregor, IEEE Trans. Nucl. Sci., **NS-56**, 742 (2009).

[27] R. Dahal, K. C. Huang, J. Cliton, N. LiCausi, J.-Q. Lu, Y. Danon, and I. Bhat, Appl. Phys. Lett. **100**, 243507 (2012).

[28] N. Alem, R. Erni, C. Kisielowski, M. D. Rossell, W. Gannett, and A. Zettl, Phys. Rev. B**80**, 155425 (2009).

[29] L. Song, L. Ci, H. Lu, P. B. Sorokin, C. Jin, J. Ni, A. G. Kvashnin, D. G. Kvashnin, J. Lou, B. I. Yakobson, and P. M. Ajayan, Nano Lett. **10,** 3209 (2010).

[30] C. R. Dean, A. F. Young, I. Meric, C. Lee, L. Wang, S. Sorgenfrei, K. Watanabe, T. Taniguchi, P. Kim, K. L. Shepard and J. Hone, Nat. Nanotechnology **5**, 722 (2010).

[31] A. K. Geim and I. V. Grigorieva, Nature **499**, 419 (2013).

[32] S. Majety, J. Li, X. K. Cao, R. Dahal, B. N. Pantha, J. Y. Lin, and H. X. Jiang, Appl. Phys. Lett. **100**, 061121 (2012)
[33] H. X. Jiang, and J. Y. Lin, Semicon. Sci. Technol. **29**, 084003 (2014),
[34] X. Z. Du, J. Li, J. Y. Lin, and H. X. Jiang, Appl. Phys. Lett. **106**, 021110 (2015).
[35] L. F. Voss, C. E. Reinhardt, R. T. Graff, A. M. Conway, R. J. Nikolic´, N. Deo, and C. L. Cheung, J. Electron. Mater. **39**, 263 (2010).
[36] S. Grenadier, J. Li, J. Y. Lin, and H. X. Jiang, J. Vac. Sci. Technol. A **31**, 061517 (2013).
[37] A. Many, J. Phys. Chem. Solids **26,** 575 (1965).
[38] Y. Nemirovsky, A. Ruzin, G. Asa, and J. Gorelik, J. Electronic Materials, **25**, 8 (1996).
[39] P. R. Wallace, Phys. Rev. **71**, 622 (1947).
[40] G. W. Semenoff, Phys. Rev. Lett. **53**, 2449 (1984).
[41] X. K. Cao, B. Clubine, J. H. Edgar, J. Y. Lin, and H. X. Jiang, Appl. Phys. Lett. **103**, 191106 (2013).
[42] J. Clinton "Optimization and Characterization of a Novel Self Powered Solid State Neutron Detector," Doctoral Thesis, Rensselaer Polytechnic Institute, Chap. **3**, 73–78 (2011).
[42] T. C. Doan, J. Li, J. Y. Lin, H. X. Jiang, AIP Advances, to be published.
[43] A. Maity, T. C. Doan, J. Li, J. Y. Lin, H. X. Jiang, Appl. Phys. Lett., to be published.